Multivariate analysis of bar fractions in the local Universe

Author: Guillem Merino Muñoz.
Facultat de Física, Universitat de Barcelona, Diagonal 645, 08028 Barcelona, Spain.

Advisor: Dr. Josep Maria Solanes

Abstract: This study presents a detailed investigation of bar abundances in present-day disk galaxies partitioned into morphological and activity classes. The relationship between bar fractions, and both the stellar mass and local environmental density of the galaxies has been examined using data from the literature that rely on two different bar identification procedures applied to objects extracted from two Sloan surveys, one based on SDSS and the other on MaNGA observations. Our study reveals that galaxies of all Hubble and BPT types show a more or less pronounced tendency to exhibit higher bar fractions with increasing stellar mass, being, respectively, the Sc and Seyfert galaxy classes the ones in which these transient structures are more abundant. We also detect two distinct regimes in the behaviour of the bar fraction with this parameter that, we speculate, could be related to the golden mass of galaxy formation. In contrast, the bar fraction is found to exhibit a weak or negligible dependence on the local baryon density. Although the results inferred from the two catalogues analysed show an overall consistency, there are some discrepancies in the behaviour of the predicted bar fractions, more obvious in the high-mass regime, that can hardly be explained unless there are hidden biases in the selection functions of the datasets

I. INTRODUCTION

The study of bar fractions has been a significant focal point for astrophysicists and cosmology researchers in recent years due to their pivotal role in galaxy formation and evolution. Understanding these structures is crucial for comprehending the dynamics of galaxies and the distribution of matter within them. Bar fractions are believed to aid in the redistribution of baryonic mass and angular momentum of galaxies over time, ultimately leading to the formation of permanent structures such as bulges and disks. In pursuit of this understanding, astronomers have amassed a wealth of information on numerous galaxies, organizing their properties into catalogues and surveys accessible to readers online. In this paper, we utilize the final release of the MaNGA PyMorph Photometric and Deep Learning Morphological catalog [1] to present updated findings on the dependence of bar fraction on stellar mass and environmental density, building upon the results of previous studies.

We aim to comprehensively analyze the abundance of the bar fraction in disk galaxies. Our motivation is to gain a deeper understanding of the factors influencing bar formation and to identify any correlations with various galaxy properties. To achieve this, we employ the outcome of machine learning algorithms trained using distinct bar identification methods. These models are applied to observational data collected from the local volume of the Universe, allowing us to explore potential variations in bar fraction abundances.

To provide a detailed characterization of bar populations, we adopt two classification schemes: morphological types and the BPT-NII (Baldwin-Phillips-Terlevich [2]) activity types. The morphological classification divides galaxies into distinct types, such as early-type disks ($S0$) and late-type spirals (Sa, Sb, Sc), while the BPT diagram provides insights into the ionization mechanisms and activity levels within galaxies. By incorporating these classification schemes, we can investigate how bar fractions vary across different galaxy populations.

Our methodology involves analyzing the relationship between bar fraction and two galaxy properties, one intrinsic and one extrinsic, namely stellar mass and baryonic local density. Stellar mass is perhaps the most fundamental intrinsic property of galaxies and the main driver of their evolution, and serves as a fundamental indicator of the overall mass within galaxies, allowing us to examine how bar fraction evolves as a function of mass. Local density, on the other hand, will provide insight into the environment of galaxies, enabling us to explore the dependence of galaxy property on the surrounding matter.

II. DATA AND METHODOLOGY

The extended version NSA catalogue comprises approximately 630,000 galaxies and contains an extensive set of approximately 90 properties for each galaxy. However, our study focuses on only two specific properties that are relevant to the dependence of bar fraction, among them the local baryonic density, percentiles, and stellar mass. The data obtained for the former was provided by the advisor of this study, whereas information on the latter from the GALEX-SDSS-WISE Legacy Catalog 2 [4]. The selection of these properties is based on previous studies that have explored the relationship between bar fraction and these specific variables. By comparing our new results with these previous findings, we can effectively highlight the discrepancies between catalogues.

For the NSA plots, we have considered as statistically valid only bins that contain 30 or more galaxies. The width of these bins is set at 0.4 for the stellar mass study

while a narrower range width of 0.2 is used for the density percentile.

The extended NSA catalog assigns bar probability values, obtained from SDSS-DR7 (Sloan Digital Sky Survey [3]), using machine learning techniques trained on either the N10 or the GZ2 samples. Consequently, we will obtain two distinct bar fraction values denoted as $F^{\rm SDSS}_{\rm bar,\ N10}$ and $F^{\rm SDSS}_{\rm bar,\ GZ2}$, which will be subsequently compared.

The N10 catalog, conducted by the professional astronomers Nair & Abraham in 2010, is a gathering of various properties of ~ 10000 nearby galaxies, including the presence or absence of a bar. This catalog has served as a training dataset for assessing the morphology and assigning a bar probability for each galaxy in the SDSS.

Likewise, the GZ2 survey determines the presence of a bar through a statistical analysis of choices made by volunteer citizens who were asked to identify these structures in the same SDSS dataset. As a result, we anticipate that bar fractions will be larger when using the N10 bar probability estimator. Professional astronomers are more adept at identifying subtle bars compared to amateur astronomers, who were only instructed to identify prominent ones. The GZ2 catalog has been employed as a training sample to estimate the bar probability for both SDSS and MaNGA galaxies.

The second catalogue we use to estimate bar fractions is MaNGA. For this smaller catalogue, statistically valid bins are considered those with a minimum of 10 galaxies. The range width for stellar mass is set at 0.4 units, whereas for the case of percentile, the range width is 0.2 units. MaNGA also offers bar probability estimates for each galaxy through machine learning analysis using only the GZ2 as training sample, that brings out another bar fraction value denoted as $F^{MAN}_{bar,GZ2}$.

In our study, a galaxy is classified as barred when the provided bar probability value exceeds the threshold of $P_{\rm bar} = 0.5$. Note that elliptical galaxies must be excluded from the present analysis as they lack a disk component. Since they can be easily confused with $S0$ galaxies, the machine learning evaluation assigns a probability to any early type object to be classified as S_0, denoted as P_{S0}. Only galaxies with $P_{S0} > 0.7$ have been included in the statistical analysis.

In order to compute the bar fractions of local galaxies we use the following formula, which produces slightly biased estimates of the mean values but in exchange provides very good estimates of the associated errors, especially for extreme values of the fractions:

$$f = \frac{N_s + 0.5z^2}{N}. \tag{1}$$

Here z stands for the standard deviation and has been taken equal to 1, providing the 68% confidence interval, and N and N_s are the total number of galaxies and the number of barred galaxies for each bin, respectively. The error per bin is given by

$$\delta f = \frac{z}{N + z^2}\sqrt{\frac{N_s}{N(N - N_s)} + \frac{z^2}{4}}. \tag{2}$$

III. DISCUSSION

We have investigated the relationship between the bar fraction, stellar mass and density percentile in the MaNGA catalogue. Additionally, we have compared our findings with the results predicted for the SDSS catalog. Figure 1 displays our results for the entire survey sample, as well as the breakdown according to different morphology types.

A. Morphology Type Classification

1. *Stellar Mass*

Regarding the stellar mass dependence, it is evident that the observed trends are consistent across all three bar fractions. The plots clearly demonstrate that stellar mass strongly influences the bar fraction, confirming findings from previous studies. In line with expectations, the bar fraction is highest among Sc galaxies across the entire stellar mass range, followed by Sb, Sa, and $S0$ galaxies, respectively.

However, notable differences are observed in the shapes of the stellar mass curves, particularly in the lower mass region. It is important to emphasize the significance of the overall bar fraction, as it visually illustrates the abundance of different galaxy types in each bin. In this regard, early type galaxies are more prevalent in lower mass bins, while later type galaxies dominate in higher mass bins.

The GZ2 panel reveals that the bar fraction exhibits a two differentiate range behaviour, shaping with a peak occurring at approximately $\log M_{\rm star} \sim 9.2$ and reaching a saturation value at $\log M_{\rm star} \sim 11.2$ for the total sample of galaxies. This two-fold behaviour becomes more apparent as galaxies disk component becomes more relevant. Furthermore, more prominent slopes are observed for stellar mass values around $\log M_{\rm star} \sim 10.4$, suggesting the presence of additional mechanisms influencing bar formation in galaxies beyond this threshold. However, this portion of the function eventually reaches a peak, indicating a saturation value for stellar mass in relation to bar formation.

Upon examining the N10 plot, it is confirmed that the previous tendency observed in the GZ2 plot holds true for the total bar fraction. However, this dual behavior is not observed in the subdivision based on morphology types. Instead, a separate study can be conducted for distinct mass regions. Specifically, $S0$, Sa, and Sb galaxies exhibit a similar pattern, characterized by a relatively constant shape in the lower mass region, followed by a substantial increase in the function slope

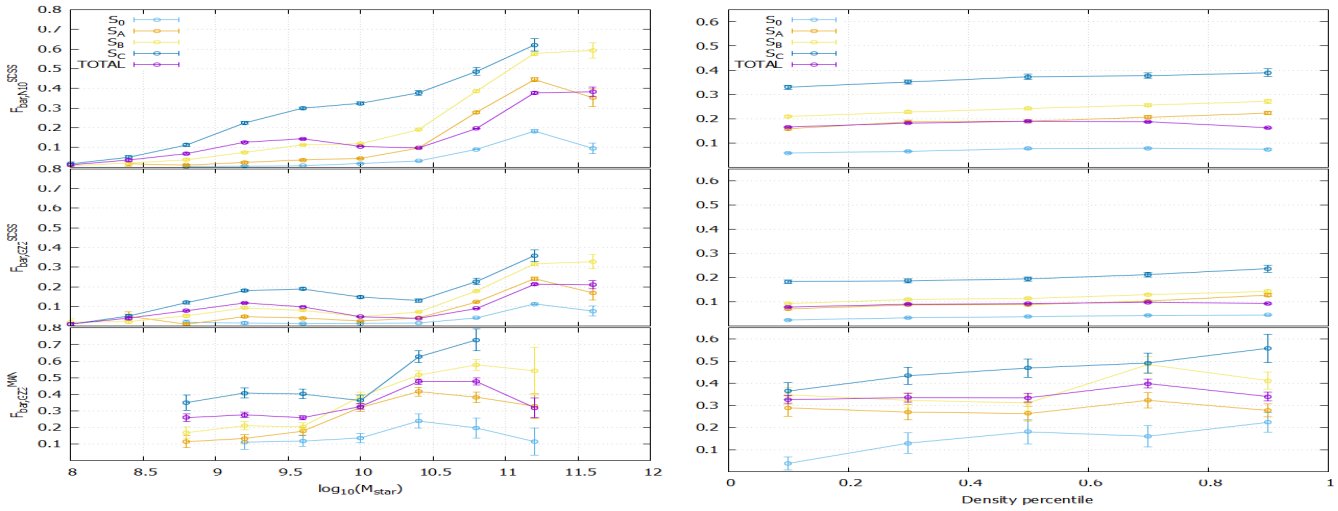

FIG. 1: Total and morphological splitted bar braction as a function of stellar mass (left) and density percentile (right) for the different bar estimations N10 and GZ2, applied to SDSS and MaNGA catalogues.

around $\log M_{\rm star} \sim 10.2$. Similar to the GZ2 plot, a saturation peak is reached for stellar masses close to $\log M_{\rm star} \sim 10.4$.

On the other hand, *Sc* galaxies show a more continuous evolution of the bar fraction with respect to stellar mass. In the lower mass range, the fraction rapidly increases and appears to reach a turning point around $\log M_{\rm star} \sim 10$, indicating the influence of other mechanisms in this mass range. Beyond this point, the slope of the function increases once again.

The MaNGA data exhibits a distinct behaviour compared to the previous plots. In this case, the bar fraction remains nearly constant for the low mass range, then gradually increases in the 9.6 to 10.4 stellar mass range, reaching a peak in around this latter value and decreasing again for larger stellar masses. This suggests that, for the observed total sample of galaxies, earlier galaxies are more likely to have higher stellar masses.

These findings highlight the importance of considering the specific dataset and observational sample when studying the relationship between stellar mass and bar fraction, as different patterns are observed for all different bar models. However, from the analysis of this graph, two general behaviors can be observed in the dependence of the bar fraction on stellar mass, dividing the lower and larger stellar mass regions.

In the lower stellar mass region, the bar fraction exhibits a practically constant behavior across all subclassifications. This contrasts with the GZ2 data, which suggested a smooth dependence reaching a peak in this domain, and the N10 data, which showed a clear evolution for *Sc* galaxies. In the larger stellar mass region, the slopes of the bar fraction significantly increase, consistent with the patterns observed in the previous plots. However, in the MaNGA data, a peak emerges for the total population of galaxies, for which the saturation value previously observed disappears. Differences between the selection function of the SDSS and MaNGA datasets may explain this inconsistency.[5] It is important to note that the uncertainty in the data prevents a rigorous quantitative interpretation of this phenomenon.

Interestingly, these two regions are separated by a value of approximately $\log M_{\rm star} \sim 10.5$, which aligns well with the so-called stellar Golden Mass. This mass value is of significant interest in astrophysics literature, as it is associated with differences in the formation mechanisms that can also influence bar formation. Notably, all three panels demonstrate this feature, with an increase in bar formation occurring substantially from around this stellar Golden Mass value.

It is important to highlight the significant quantitative variations in bar fraction predictions observed among these different plots. These differences can be as large as 100% in the large mass region for practically all five functions when comparing the N10 panel to the GZ2 panel. Similarly, notable differences can be observed in the low mass range when comparing the MaNGA data to the others.

These variations can be attributed to several factors. Firstly, the differences in the methods used to determine whether a galaxy is barred or not for the GZ2, N10 bar models play a crucial role. Additionally, it is possible that bars in closer galaxies can be more easily distinguished than those in more distant galaxies, leading to variations in the observed bar fraction.

2. Percentile

Density percentile is calculated from an optimised version of the k-nearest neighbour Bayesian estimator (cf. Casertano & Hut 1985) that considers the average pro-

jected distance to the 5th closest neighbours from the target galaxy selected among those companions with a recessional velocity within 1000 km/s calculated in the deepest volume-limited subset that can be defined for the central object in the $z < 0.1$ region of the SDSS Legacy Survey, corrected for the effects of Galactic interstellar extinction.

In general, all three panels in figure 1 exhibit a similar overall appearance, leading to equivalent conclusions. The order of galaxy types remains consistent, with Sc galaxies displaying the highest bar fraction and decreasing as we move towards $S0$ galaxies.

Both the N10 and GZ2 plots show that bar fraction is not strongly correlated with density, if at all, in contrast to the case of stellar mass. However, slight growth is present for all subsets. The main difference between these two plots lies in the quantitative values of bar fraction. Again, the results for the MaNGA subset presents some differences. While the overall bar fraction trend remains relatively constant, both Sc and $S0$ galaxies show more obvious gradual increase with baryonic density. Similarly to total bar fraction function, Sb galaxies appear to exhibit a constant trend for density values below approximately 0.5, but a peak is observed near 0.7. This behavior seems to be replicated by Sa galaxies as well.

B. BPT Classification

The MaNGA and SDSS datasets are divided into three distinct activity classes, namely star-forming galaxies, composite galaxies, and active galactic nuclei (AGN) galaxies, obtained from Thomas et al. (2013). Figure 2 shows the results for this case, through which we have analyzed the total bar fraction dependence, which should exhibit a similar pattern to that observed in morphology classification.

1. Stellar Mass

In the BPT splitting analysis, the obtained fractions exhibit greater similarity compared to the previous case. In the N10 panel, the total bar fraction curve reaches a peak around $logM_{star} \sim 9.5$ before rapidly increasing slopes, eventually reaching a saturation value at $logM_{star} \sim 11$. This is consistent with our results from morphological classification, where a peak was observed in the low mass range followed by increased slopes. The total bar fraction curve closely resembles the behavior of star-forming galaxies for the low mass range, although AGN's seem to compound the majority of galaxies for the large mass region. For composite and AGN galaxies, the behavior in the large mass range is similar to that of the total bar fraction mentioned, while the low mass range displays a constant bar fraction.

The GZ2 plot closely resembles the N10 panel, with the total and star-forming bar fraction curves exhibiting almost identical behavior. The AGN curve also shows a similar pattern. The main difference lies in the predicted values of bar fraction abundances.

The MaNGA results, however, significantly differ from the values obtained for the N10 and GZ2 subsets. In this case, the total bar fraction function remains constant in the low mass range and reaches a saturation value in the large mass range, increasing rapidly from $logM_{star} \sim 9.5$ to $logM_{star} \sim 10.5$. Once again, the behavior of star-forming galaxies closely resembles this pattern for low masses and AGN's take importance in large mass range. AGN galaxies exhibit clear growth with stellar mass, maintaining a roughly constant slope and dominating the behavior of the total bar fraction in the high-mass range. The same growth trend is observed for composite galaxies, although their fraction remains constant in the low mass range.

2. Percentile

The percentile figures exhibit truly similar shapes compared to the morphology splitting. The constant behavior is confirmed in these plots, with minor variations in bar fraction values of around ~ 0.1. In the GZ2 and N10 plots, the clear order is maintained, with composite galaxies having the highest percentage of barred galaxies, followed by AGNs and star-forming galaxies, respectively. The curves of composite galaxies and AGNs overlap for some percentile values, although uncertainties cover the regions where these functions intersect, particularly in the GZ2 data.

The MaNGA plot generally reproduces these results, although a couple of discrepancies are observed. In this case, composite galaxies have the lowest population of barred galaxies, even though the constant shape is practically maintained. AGN's seem to exhibit a slight peak for medium values of the percentile, although it is not pronounced and the constant shape is still within the range of uncertainties.

IV. CONCLUSIONS

Bar fraction evolution has been studied using two indicators of galaxy properties and two distinct bar models derived through machine learning. These models were trained using two different methods for bar identification. One of them has been applied to two different catalogues whereas the other to only one. Additionally, two subclassifications based on morphology types and the BPT diagram splitting were employed to enhance our understanding of bar populations and the associated classifications relevant to the presence of bars in galaxies.

In this regard, an initial observation can be made regarding the similarity of the BPT curves, with the exception of the stellar mass plot. Notably, the low

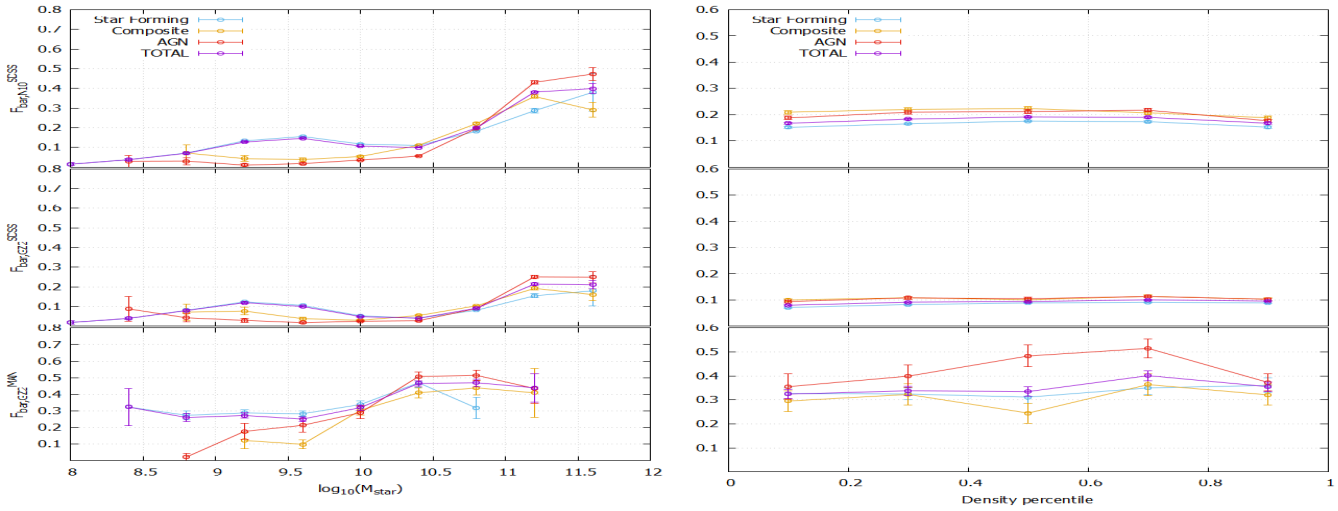

FIG. 2: Total and activity splitted bar braction as a function of stellar mass (left) and density percentile (right) for the different bar estimations N10 and GZ2, applied to SDSS and MaNGA catalogues.

mass range behavior of AGN and composite galaxies exhibits significant differences compared to other subtypes. AGN galaxies tend to have a higher population of barred galaxies, followed by composite and star-forming galaxies. This contrasts with the morphology-based classification, where distinct subsets exhibit notable variations in shapes and quantitative values. Specifically, Sc galaxies demonstrate the highest bar fraction, followed by Sb, Sa, and $S0$ galaxies, thereby corroborating previous findings on this topic.

Despite notable quantitative differences, the overall trends remain consistent between the N10 and GZ2 bar models across various galaxy properties, with some variations primarily observed in the stellar mass subtype functions within the morphology subdivision. However, the introduction of new observations from the MaNGA dataset has yielded distinct results, which have both confirmed and refined previous observations, thereby enhancing our understanding of bar formations. Notably, MaNGA has unveiled novel behaviors in the overall bar fraction patterns or specific ranges of values for all three property indicators, offering fresh insights into interpretations, threshold values, and saturation points that were previously unexplored.

It has been established that there is a confirmed correlation between the presence of bars and stellar mass, with an increasing bar population observed for higher stellar mass values, typically beginning around $logM_{star} \sim 10$ and approaching a saturation point for larger masses. Interestingly, when examining the low mass region, the analysis of MaNGA data has revealed a new behavior characterized by a constant bar fraction, which contrasts with earlier findings that indicated a peak in this particular range.

The analysis of bar fraction in relation to galaxy density, as confirmed by the MaNGA dataset, suggests that bar fraction is not strongly influenced by density. While a smooth dependence on density may be present, particularly observed in Sc and $S0$ galaxies, these findings contrast with the indications from N10 and GZ2 studies. However, it is important to note that there is a significant level of uncertainty associated with these results, raising the possibility that these observed tendencies may not be entirely reliable. Furthermore, the examination of BPT indicators does not support the notion of bar fraction exhibiting a growth pattern tied to density.

Acknowledgments

I would like to thank my advisor, Josep Maria Solanes, for his guidance and patience through this project.

[1] MaNGA Morphology Deep Learning DR17 catalog, Domínguez Sánchez et. al. 2021 MNRAS 509 3
[2] Classification parameters for the emission-line spectra of extragalactic objects, J. A. Baldwin et al 1981 PASP 93 5
[3] Improving galaxy morphologies for SDSS with Deep Learning, Domínguez Sánchez et al. 2018 MNRAS 476 3661-3676
[4] GALEX-SDSS-WISE Legacy Catalog 2, Salim et al. 2018 ApJ 11 17
[5] Regrettably, we lack the necessary information to weight the data and compensate for them.